

ACOUSTIC CYCLOTRON RESONANCE IN AN INCLINED MAGNETIC FIELD IN ANTIMONY

A. P. KOROLYUK, L. Ya. MATSAKOV and V. L. FAL'KO

Institute of Radiophysics and Electronics, Academy of Sciences, Ukrainian S.S.R.

Submitted May 5, 1967

Zh. Eksp. Teor. Fiz. 54, 3-15 (January, 1968)

Acoustic cyclotron resonance (ACR) in antimony situated in a magnetic field \mathbf{H} inclined with respect to the sound wave vector \mathbf{k} is investigated. The anisotropy of the ACR periods is studied experimentally for various orientations of \mathbf{k} and \mathbf{H} with respect to the crystallographic axes. The effective masses and the mean drift velocities of the carriers along the magnetic field on the boundary cross sections of the Fermi surface are determined from the Doppler splitting. The shape of the ACR lines, the periods of oscillation, effective masses and mean drift velocities of the carriers along the magnetic field are calculated on the basis of the anisotropic quadratic dependence of the antimony Fermi surface. It is shown that there is qualitative agreement of the experimental results with the theoretical calculations, although the quantitative agreement is not always satisfactory. Some causes of the quantitative divergence between experiment and theory is discussed.

INTRODUCTION

The study of the features of ultrasonic absorption in a metal is an effective method for the study of the energy spectrum of quasiparticles. The interaction of a sound wave with the conduction electrons in the absence of an external constant magnetic field leads to oscillations in the sound absorption coefficient—magnetoacoustic resonances. It is not difficult to understand the physical nature of these resonances. The sound oscillations create a spatially periodic field in the metal. In the presence of a sufficiently strong magnetic field \mathbf{H} , the sound absorption is produced by separate groups of “effective” electrons, on whose trajectories are the points

$$k\mathbf{v} = \omega \quad (1.1)$$

(\mathbf{k} and ω are the wave vector and the sound frequency, \mathbf{v} the velocity of the electrons). Near these points the electrons move in phase with the wave and absorb its energy effectively. The magnetoacoustic resonances arise if the characteristic dimension of the electron trajectory in the magnetic field is a multiple of the “spatial period” of the sound wave. The variety of the magnetoacoustic resonances is associated with the existence of a large number of different mechanisms of selection of the effective electrons.

In a magnetic field \mathbf{H} perpendicular to the direction of propagation of sound, all the electrons on closed orbits of the Fermi surface are effective. The geometric

(Pippard) resonance observed in this case is due to the separation of electrons with extremal diameters.^[1] In the high frequency region,

$$\omega \gg v \quad (1.2)$$

the oscillations of the geometric resonance are modulated by the acoustic cyclotron resonance at the multiple frequencies $\omega = n\Omega$ ^[2] (ν is the frequency of electron collisions, Ω the cyclotron frequency; $n = 1, 2, 3, \dots$ is an integer).

In the presence of drift motion of the electrons along the wave vector \mathbf{k} , the electrons satisfying the condition for resonance interaction with the sound are those for which

$$|\omega - k_{\zeta} \bar{v}_{\zeta}| = n\Omega. \quad (1.3)$$

The bar denotes averaging over the period $2\pi/\Omega$, the axis $\zeta \parallel \mathbf{H}$. In the quasistatic region of frequencies

$$\omega \ll v \quad (1.4)$$

the sound frequency can be neglected and Eq. (1.3) is rewritten in the form

$$u(p_{\zeta}) = n\lambda \quad (n = 0, 1, 2, \dots). \quad (1.5)$$

Here $u(p_{\zeta}) = |2\pi\Omega^{-1}\bar{v}_{\zeta} \cos \varphi|$ is the absolute value of the displacement of the electron along the vector \mathbf{k} after one period, p_{ζ} is the projection of the momentum; φ is the angle between the vectors \mathbf{k} and \mathbf{H} . Consequently, the resonance interaction with the sound exists for those

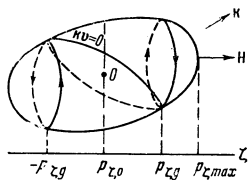


FIG. 1. Boundary trajectories of electrons and the lines $k \cdot v = 0$ of the convex closed Fermi surface.

electrons whose displacements are multiples of the wavelength λ . In the case of strong spatial dispersion, $u \gg \lambda$ and a large number of different resonant groups exist.

The mechanism of selection of the electrons can be connected with the features of their energy spectrum—the sharp departure of the Fermi surface from ellipsoidal^[3,4] and the presence of open surfaces.^[5] In metals with a closed convex Fermi surface, electrons belonging to the boundary cross sections are separated (Fig. 1).^[4] These cross sections divide the effective and ineffective electrons. Change in the magnetic field H leads to a change in the number of resonance states, i.e., a group of resonance electrons appears or disappears in the interval $-p_g < p_\zeta < p_g$ (Fig. 1). The sound absorption coefficient Γ will experience periodic increases for values of the magnetic field H satisfying the condition

$$u(p_g) = n\lambda. \quad (1.6)$$

In the region of high sound frequencies (1.2) splitting into two is characteristic of the absorption lines, since the Doppler frequency shift is different for electrons with oppositely directed velocity projections in the direction of the wave vector k .

Magnetoacoustic resonances due to electrons on the boundary cross sections were predicted theoretically by Kaner, Peschanskiĭ and Privorotskiĭ^[2-4] and were discovered experimentally by us in antimony.^[6] The splitting of the resonance lines was observed in antimony at the sound frequency $\omega/2\pi = 5.0 \times 10^8$ Hz.^[7] The oscillation of the sound absorption in arsenic and antimony, which was reported in the work of Eckstein,^[8] must be ascribed to effects of the same type. However, the latter author connected these absorption features with electrons close to the elliptical limiting points on the Fermi surface. However, as was pointed out earlier,^[9] the electrons near the limiting points are not effective and do not lead to any resonance oscillations.

In the present work, resonance oscillations have been studied in detail at the boundary cross sections in antimony. By their nature they are acoustic cyclotron resonances (ACR) at frequencies that are shifted by virtue of the Doppler effect. The experimental results are compared with theoretical calculations carried out under the assumption of an anisotropic quadratic model of the Fermi surface of antimony.

2. THEORY

The theoretical analysis of the magnetoacoustic resonance effects in an oblique magnetic field for metals with multi-connected convex Fermi surfaces was carried out by Kaner and one of the authors.^[9] The region of magnetic fields considered is sufficiently strong that the inequality

$$1 \ll kR \ll kl \quad (2.1)$$

is satisfied (R is the characteristic radius of electron trajectories in the magnetic field, l the free path length). It was shown that the magnetoacoustic resonances in an oblique magnetic field, over a wide range of angles of inclination θ (different from $\pi/2$), were due to the drift motion of the electrons close to the boundary cross sections of the Fermi surface. Electrons from the vicinity of limiting points, as a consequence of their ineffectiveness, lead only to separate singularities of the sound absorption coefficient, of the type of "edge absorption" of Kjeldaaas.

In what follows, we shall consider a semimetal with a quadratic anisotropic dispersion law for the electrons:

$$\varepsilon_\alpha = 1/2 (\hat{p} \hat{\mu}_\alpha^{-1} \hat{p}). \quad (2.2)$$

Here α is the number of carrier groups, ϵ the Fermi energy of the electrons, $\hat{\mu}$ the effective mass tensor.

In the propagation of ultrasound in metals in an oblique magnetic field (2.1) an unusual "quantization" of the electron states takes place, brought about by the resonance character of the interaction of the electrons with the sound wave (1.5). As a result, the sound absorption coefficient Γ is a sum over discrete "quantum" states:

$$\Gamma = \sum_\alpha \Gamma_\alpha^{(\omega)} [1 + \beta \alpha^2(\theta) \text{tg}^2 \theta]^{1/2} \sum_{|n| \leq |k_\zeta \rho|} J_n^2 [\beta(\theta) \text{tg} \theta (k_\zeta^2 \rho^2 - n^2)^{1/2}]. \quad (2.3)$$

Here $J_n(z)$ is the Bessel function, n an integer, $2\pi\rho = 2\pi\bar{v}_\zeta \zeta_{\max}$ is the maximum shift in the direction of the magnetic field H ; the quantity

$$\beta(\theta) = [(h\hat{\mu}h)(q\hat{\mu}^{-1}q) - \cos^2 \theta]^{1/2} / \sin \theta \quad (2.4)$$

describes the anisotropy of the ellipsoid and is equal to the ratio of the central diameter to the quantity 2ρ : $h = H/H$, $q = k/k$ are unit vectors; $\Omega = eH/mc$ is the cyclotron frequency;

$$m = \frac{1}{2\pi} \frac{\partial S(\varepsilon, p_\zeta)}{\partial \varepsilon} = \left(\frac{h\hat{\mu}h}{\det \hat{\mu}} \right)^{-1/2} \quad (2.5)$$

is the cyclotron mass; $\det \hat{\mu}$ is the determinant of the matrix μ_{ijk} , $S(\varepsilon, p_\zeta)$ is the cross section of the Fermi surface in the plane $p_\zeta = \text{const}$;

$$\Gamma_0^{(\alpha)} = \frac{2\pi^2}{(2\pi\hbar)^3 W} \frac{|g_\alpha^2| (h\hat{\mu}_\alpha h)}{k [\cos^2 \theta + \beta \alpha^2(\theta) \sin^2 \theta]^{1/2}}$$

is the sound absorption coefficient of the α carrier group in the absence of a magnetic field, W is the flux density of the sound wave; $g = -i\omega \Lambda_{ijk}(0) u_{ijk}$, Λ_{ijk} are the components of the deformation potential tensor, and u_{ijk} the amplitude value of the deformation tensor. (Justification for taking into account only the deformation contribution to the sound absorption for semimetals is given in^[9].)

Equation (2.3) is an exact expression for the absorption coefficient of a plane monochromatic sound wave in a wide range of angles of inclination ϑ and magnetic fields H , satisfying the condition

$$\frac{(2\gamma)^{3/2}}{(k\rho)^{1/2}} \frac{(\beta \sin \theta)^{1/2}}{(\cos^2 \theta + \beta^2 \sin^2 \theta)^{1/2}} \ll \cos \theta \quad (2.6)$$

(the parameter $\gamma = \nu/\Omega \ll 1$ characterizes the purity of the metal).

In a narrower range of angles of inclination ϑ , restricted by the criterion

$$\cos \vartheta < \left(\frac{8}{k_{\zeta} \rho}\right)^{1/2} \frac{(\cos^2 \vartheta + \beta^2 \sin^2 \vartheta)^{1/2}}{(\beta \sin^2 \vartheta)^{1/2}}, \quad (2.7)$$

and for not too strong magnetic fields, when the value of $k_{\zeta} \rho$ is large:

$$k_{\zeta} \rho \gg 1, \quad (2.7')$$

the magnetoacoustic resonances are described by the asymptotic formula

$$\Gamma = \sum_{\alpha} \Gamma_{\alpha}^{(a)} \{1 + 2[1 + \beta^2(\vartheta) \text{tg}^2 \vartheta]^{1/2} J_{n_0}^2[\beta(\vartheta) \text{tg} \vartheta (k_{\zeta}^2 \rho^2 - n_0^2)^{1/2}]\}. \quad (2.8)$$

Here n_0 denotes the integral part of the quantity

$$x \equiv \frac{k u(p_g)}{2\pi} = \frac{k_{\zeta} \rho \beta \text{tg} \vartheta}{(1 + \beta^2 \text{tg}^2 \vartheta)^{1/2}}.$$

Separation of the principal component with $n = n_0$ from the sum (2.3) is due, from the physical point of view, to the difference between the effective and the ineffective electrons. Account of the ineffective electrons, which are determined by terms with $n > n_0$, leads to insignificant, exponentially small corrections. The sound absorption coefficient Γ experiences a sharp periodic increase as a function of the parameter $x = k u(p_g)/2\pi$, inversely proportional to the value of the magnetic field. The period of these increases is determined by the condition $\Delta x = 1$ and is connected with the value of the drift velocity of the electrons near the boundary cross sections:

$$\Delta(1/H) = e / k c m \bar{v}_{\zeta}(p_g) \cos \vartheta, \quad (2.9)$$

$$\bar{v}_{\zeta}(p_g) = v_{\zeta \max} \left[\frac{(\hbar \mu \hbar (\mathbf{q} \mu^{-1} \mathbf{q}) - \cos^2 \vartheta)}{(\hbar \mu \hbar) (\mathbf{q} \mu^{-1} \mathbf{q})} \right]^{1/2}.$$

It must be emphasized that the amplitude of the resonance maxima depends significantly on the parameter $\beta(\vartheta) \tan \vartheta$ and changes with change in the angle ϑ . As follows from the properties of the Bessel function, the positions of the maxima can be displaced relative to the points $x = n$, and this displacement is the more significant the smaller the value of $\beta \tan \vartheta$. Generally speaking, aperiodic oscillations exist between the principal maxima. They are described by an expression of the type

$$\psi_n(x) \equiv [2n_0(1 + \delta)]^{-1/2} \sin \varphi_{n_0-1}(x),$$

$$\psi_n(x) \equiv [(x^2 - n^2)(1 + \beta^2 \text{tg}^2 \vartheta)]^{1/2} - n \arctg \frac{[(x^2 - n^2)(1 + \beta^2 \text{tg}^2 \vartheta)]^{1/2}}{n}. \quad (2.10)$$

Here $\delta = x - n_0$. In the limiting case, expressed by Eqs. (2.7), (2.7'), the amplitude and the "period" of these oscillations are much less than the principal ones. Therefore, components of the form (2.10) are omitted in the asymptotic formula (2.8) for the coefficient Γ .

In the experimental investigation of the ultrasonic absorption coefficient, interest attaches to stronger magnetic fields, for which

$$k_{\zeta} \rho \gg 1. \quad (2.11)$$

This is connected with the fact that in comparatively weak fields (2.7'), the characteristic dimensions of the electronic trajectories R are large and in practically achievable mean free path lengths of the electron the condition $l \gg R$ (see (2.1)) does not exist. Scattering of the electrons leads to a broadening of the resonances and it becomes extremely difficult to observe them. In the region of magnetic fields (2.11), it is not possible to

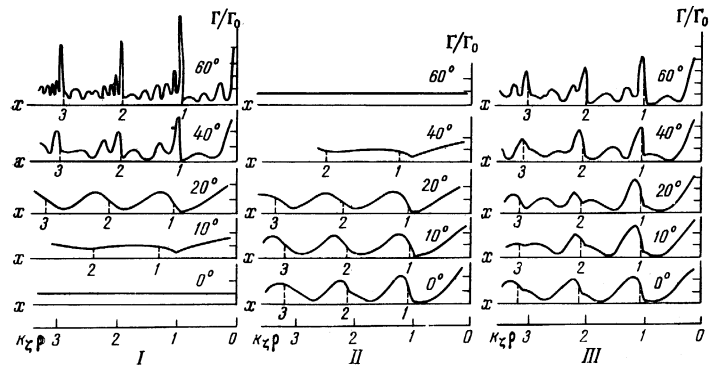


FIG. 2. Shape of the resonance oscillation lines in antimony on the boundary trajectories for electron ellipsoids, computed from the anisotropic quadratic model of the Fermi surface: I—for the principal ellipsoid, II and III—for ellipsoids rotated respectively by -120 and $+120^\circ$. The sound wave vector is parallel to the binary axis X, the vector \mathbf{H} is located in the plane of the binary and bisectric axes XY.

use the asymptotic formula (2.8). Investigation of the exact sum of (2.3) is necessary.

The exact computation of the sound absorption coefficient was carried out by us for antimony for different angles of inclination of the magnetic field \mathbf{H} relative to the vector \mathbf{k} . The case was considered of propagation of sound along the binary axis of the crystal for $\omega \ll \nu$.

As is well known,^[10,11] the Fermi surface of antimony consists of three electron and six hole surfaces, which resemble ellipsoids only in first approximation. Therefore, it is generally not possible to interpret the experimental results by starting out with a quadratic model. However, it can be used for making clear the qualitative nature of the ACR lines, at the same time recalling the approximate character of the model.

The decisive parameter of the problem is the quantity $\beta(\vartheta) \tan \vartheta$, since it controls the amplitude, width, and period of the resonances. To calculate the parameter $\beta(\vartheta) \tan \vartheta$, one must transform from the system of coordinates attached to the axes of symmetry of the ellipsoids, in which the effective mass tensor is described,^[12] to a system connected with the magnetic field \mathbf{H} . We shall not carry out the simple but tedious calculations here. We only note that, for example, for the principal electron and hole ellipsoids, the value of β does not depend on the angle and is equal to 6.77 (for the electrons) and 3.87 (for the holes) in the case in which the vector \mathbf{H} lies in the plane of the binary and trigonal axes of the crystal. (In the calculation, use was made of the value of the mass tensor for antimony from^[12].) For rotated ellipsoids, $\beta(\vartheta)$ is a complicated function of the angles.

Figure 2 shows the theoretical curves which describe the behavior of the sound absorption coefficient Γ for the electron ellipsoids for different values of the angle ϑ . The value of $x = (1 + \beta^2 \tan^2 \vartheta)^{-1/2} k_{\zeta} \rho \beta \tan \vartheta$ is plotted along the abscissa and the ratio Γ/Γ_0 along the ordinate. Similar curves are obtained for the holes. Inasmuch as it was assumed in the calculations that $\omega \ll \nu$, then the Doppler splitting of the absorption lines is absent from Fig. 2. In the high frequency region ($\omega > \nu$) one cannot neglect the value of ω in Eq. (1.3). This leads to branching of each maximum absorption as a consequence of the Doppler effect. All the principal results obtained in the case $\omega \ll \nu$ also hold in the high frequency region.

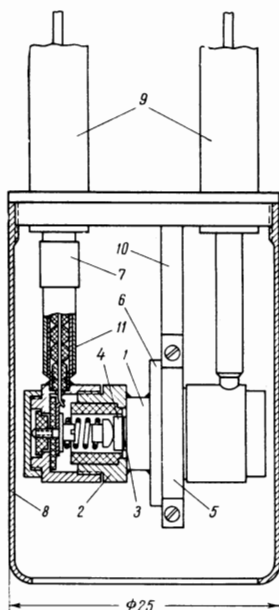


FIG. 3. Arrangement of the low-temperature part of the ultrasonic spectrometer: 1—sample under study, 2—brass washer, 3—ultrasonic transducer, 4—brass electrode, 5—fastening clamp, 6—brass washer with guiding edge, 7—coaxial connector, 8—protective container, 9—rigid coaxial line, 10—fastening brace, 11—flexible coaxial line.

In our experiments, the condition $\omega > \nu$ was satisfied; therefore, Doppler splitting of the peaks was observed for almost all orientations of the vectors \mathbf{k} and \mathbf{H} . The cyclotron mass m and the value of the mean drift velocity of the electrons \bar{v}_z close to the boundary cross sections can easily be found from the absorption line splitting by means of the formulas

$$m = \frac{ne}{c\omega} \frac{H_n^+ - H_n^-}{2}, \quad (2.12)$$

$$\bar{v}_z(p_g) = \frac{\omega}{k \cos \vartheta} \frac{H_n^+ + H_n^-}{H_n^+ - H_n^-}. \quad (2.13)$$

Here H_n^+ and H_n^- are the locations of the n -th maxima in the magnetic field for electrons drifting along the vector \mathbf{k} and in the opposite direction, respectively. Section 5 will be devoted to a discussion of the theoretical results and their comparison with experiment.

3. EXPERIMENTAL METHOD

Experiments were carried out on single crystals of antimony Su-000, treated by twenty-fold zone recrystallization ($R_{300^\circ\text{K}}/R_{4.2^\circ\text{K}} = 3 \times 10^3$).

The samples, in the shape of discs of diameter 8 mm and thickness 2–3 mm, were cut by means of an electric spark saw. The end surfaces were treated with fine abrasives until they were sufficiently plane parallel for ultrasonic measurements. Curving over the diameter of the specimen did not exceed 0.5μ or $\sim 0.05 \lambda$ (λ is the sound wavelength in antimony at $\omega/2\pi = 530$ MHz).

The measurements of ACR were carried out with a CW ultrasonic spectrometer. The parasitic power escaping from the generator to the receiver at a frequency of 530 MHz was kept down to 2–3% by careful screening. The construction of the low temperature part of the apparatus is shown in Fig. 3. The sample under study 1 was soldered to the brass washers 2 by means of Woods metal. The ultrasonic transducers were X-cut quartz crystals, attached by epoxy cement to the brass electrodes 4. The resonance frequency of the plates was 106 MHz. The fifth, seventh, and ninth harmonics were

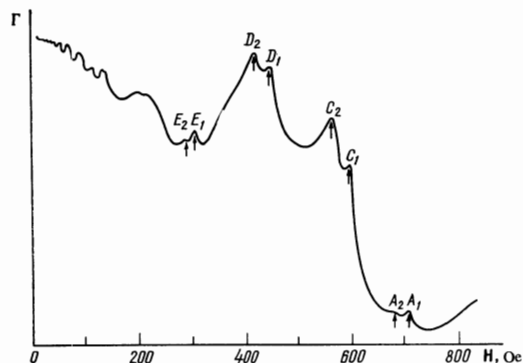


FIG. 4. Dependence of the sound absorption coefficient Γ on the value of the magnetic field H . The wave vector for sound $\mathbf{k} \parallel X$; $\vartheta = 10^\circ$. The vector \mathbf{H} is situated in the XY plane; $\omega/2\pi = 530$ MHz. The absorption peaks C_1, C_2 , and E_1, E_2 are connected with the "electron" ellipsoid II, D_1, D_2 with the electron "ellipsoid" III and A_1, A_2 —with the hole "ellipsoid" I. The splitting is produced by the Doppler effect.

used, corresponding to the sound frequencies 530, 742, and 954 MHz.

The magnetic field produced by an electromagnet could be changed with time according to a linear or hyperbolic law.^[13] In the latter case, the ACR oscillograms were obtained periodically, thus offering definite advantages in their interpretation. All the experiments were performed at a temperature of 1.3°K , produced in the cryostat by continuous pumping of the helium vapor.

4. EXPERIMENTAL RESULTS

ACR in antimony was studied in the propagation of longitudinal sound along the principal crystallographic axes in a magnetic field \mathbf{H} , which was rotated in the principal crystallographic planes containing the vector \mathbf{k} . In what follows, we shall denote the binary, bisectrix and trigonal axes by X, Y and Z , respectively. We write down the results for the case in which the wave vector \mathbf{k} is directed along the X axis and the vector \mathbf{H} is located in the planes XY or XX .

In the region of weak magnetic fields, the absorption lines are a superposition of several harmonic oscillations with small amplitude. In the strongest magnetic fields for angles of inclination $\vartheta < 30^\circ$ there are observed one, and in rare cases, two sharply split peaks (Fig. 4) produced by a definite group of carriers. It has not been possible to separate these because of the complicated picture of the beats. Therefore, we shall take as the "period" the distance in the inverse magnetic field from zero to the location of the maximum of the corresponding oscillations. The anisotropies of these "periods" in general terms should be characterized by the anisotropy of the actual periods. This allows us to connect the observed absorption lines with the corresponding ellipsoids of the Fermi surface.

In the region of larger angles $30^\circ < \vartheta < 70^\circ$, a series of several sharp absorption maxima, equidistant in the inverse magnetic field, are observed, with split vertices (Fig. 5). The determination of their periods presents no difficulty.

Similar results were obtained also for propagation of sound along the bisectrix and trigonal axes.

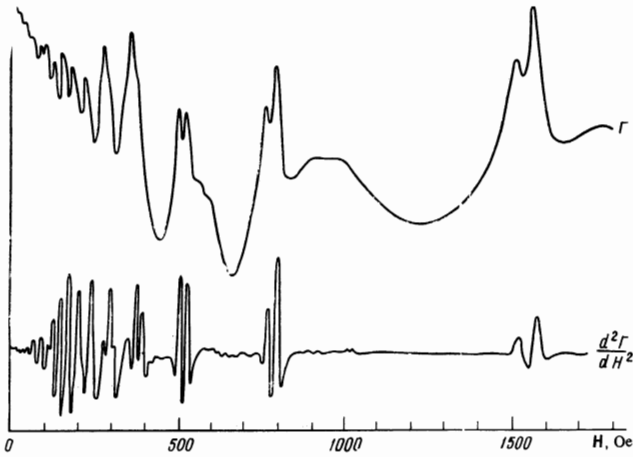


FIG. 5. Dependence of the sound absorption coefficient Γ and the second derivative of the absorption coefficient with respect to the magnet field $d^2 \Gamma/dH^2$ on the value of the magnetic field H . The sound wave vector $k \parallel X$; $\vartheta = 40^\circ$. The vector H is situated in the XY plane; $\omega/2\pi = 530$ MHz.

Figure 6 shows ¹⁾ the experimental data from the measurement of the anisotropy of the ACR periods in the propagation of longitudinal sound with frequency $\omega/2\pi = 530$ MHz along the X axis. Both the orientations of the crystallographic axes relative to the vectors k and H and the measurement of the ACR periods in the present research were done more carefully than in the preliminary communication.^[7] Figure 6a illustrates the anisotropy of the electron, and Fig. 6b, the hole periods. (In the lower curve of Fig. 6a for the XZ plane, the scale does not allow us to show the difference in the periods for the Doppler split resonance oscillations.) The solid lines in Fig. 6a and b are the results of the calculation of the periods of ACR under the assumption of anisotropic quadratic spectrum of the energy of the electrons. The values of the mass tensor were taken from^[12].

Figures 7 and 8 give the values of the cyclotron masses and the mean drift velocity of the carriers along the vector H , which are determined from the splitting of the resonance lines (see Eqs. (2.12) and (2.13)). The solid lines are the results of calculation according to the Eqs. (2.5) and (2.9). For a comparison, the crosses indicate the values of the effective masses obtained by Datars and Wanderkooy^[14] by the method of electromagnetic cyclotron resonance.

5. DISCUSSION OF RESULTS

The picture of the behavior of the absorption coefficient Γ described in the previous section agrees qualitatively with the theoretical results given in Fig. 2. At small values of the angle ϑ the theoretical curves differ essentially from sinusoidal form only at the values $x = 1$ or 2. For $x > 2$, the oscillations of the absorption co-

¹⁾Here and in all the subsequent drawings, the figures I, II and III refer to the principal ellipsoids and those rotated by -120 and $+120^\circ$, respectively.

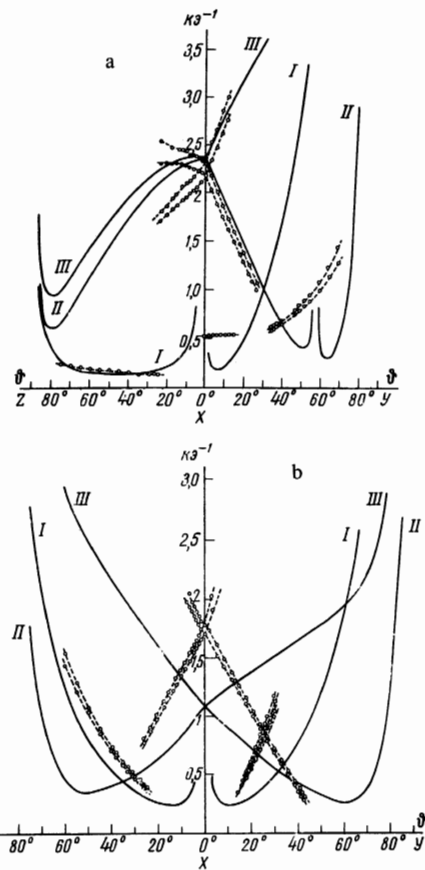


FIG. 6. Dependence of the ACR periods in an oblique magnetic field on the angle ϑ for electrons (a) and for holes (b). $k \parallel X$; $\omega/2\pi = 530$ MHz. The solid lines are computed, \circ —experimentally measured values.

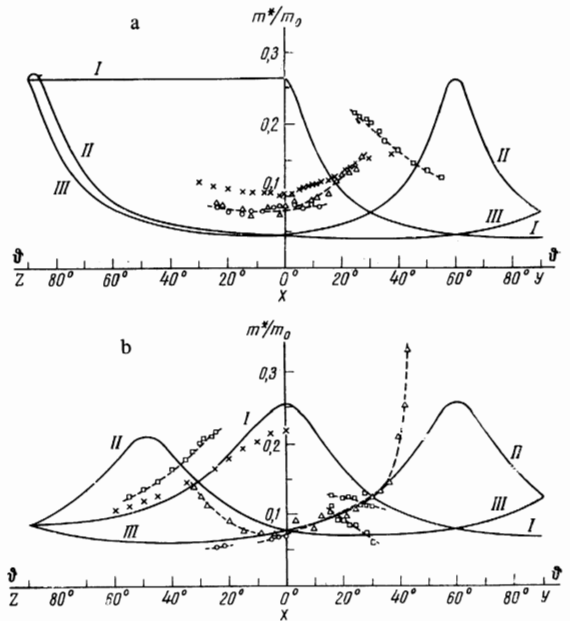


FIG. 7. Anisotropy of the cyclotron masses on the boundary cross sections for electrons (a) and for holes (b). The solid lines are computed values, X —values of the cyclotron masses from^[14].

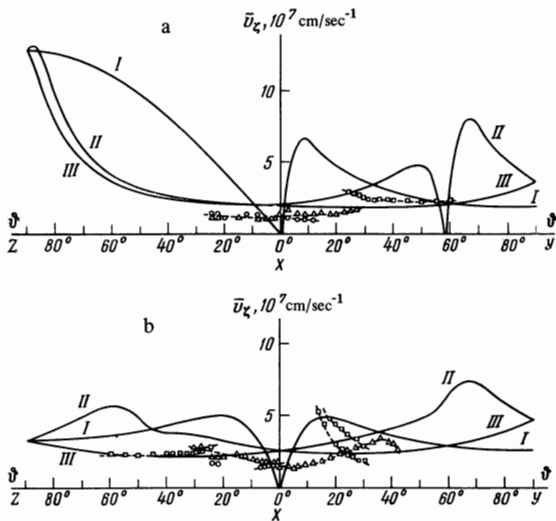


FIG. 8. Anisotropy of the mean drift velocities of the electron (a) and holes (b) along the direction of the magnetic field H on the boundary cross sections. Solid lines—computed values.

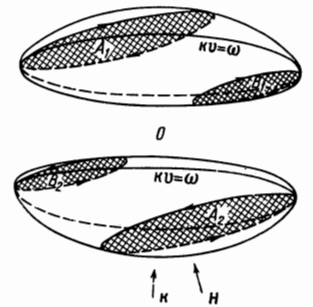
efficient Γ take the form of damped harmonic oscillations (or the superposition of several damped oscillations). Upon increase in the angle φ ($\varphi > 30^\circ$) the resonance lines corresponding to the principal (I) and one of the rotated ellipsoids (III) are sharp peaks in the broad range of angles. The oscillations brought about by the second rotated ellipsoid (II) are broadened and fall off rapidly in amplitude. In the experiment, it was not possible to track the sharp maxima connected with the rotated ellipsoid (III) at angles greater than 20° . Because of the rapid growth of the period, these oscillations fall off in the region of weak magnetic fields and the scattering of the electrons leads to a broadening of the resonances.

It follows from Fig. 2 that the maxima in the absorption are displaced relative to the points $x = n$ in the direction of larger values of x (i.e., weaker magnetic fields). This shift becomes significant only for a value of the parameter $\beta \tan \varphi < 3$, which, for example, for the principal electron ellipsoid, corresponds to angle $\varphi < 25^\circ$. For angles $\varphi > 25^\circ$, the locations of the resonance peaks are virtually identical with the integral values of x . The absence (with accuracy to within experimental error) of a phase shift for the periods of the resonance oscillations, brought about by electrons on the boundary cross sections, for angles $\varphi > 30^\circ$, was noted previously.^[6]

A common scale, in units of $k_z \rho$ is used for all curves in Fig. 2 (lower axis). A break ("absorption edge") is clearly seen in all the theoretical curves for $k_z \rho = 1$, which is associated with the noneffective electrons near the turning points. Corresponding features are not seen on the experimental curves.

Comparison of the experimentally measured anisotropy of the ACR periods with those calculated for the ellipsoidal model (Fig. 6) shows qualitative agreement of the results, although the quantitative agreement of the results, although the quantitative agreement is not always satisfactory. In the region of small angles $\varphi < 20^\circ$ one of the possible reasons for the divergence appears to be the not very exact measurement of the experimen-

FIG. 9. Boundary cross sections of the Fermi surface, consisting of two deformed ellipsoids with common center of symmetry.



tal periods. (The periods were determined as the distance from zero to the location of the first maximum along the scale $1/H$.) As is seen from Fig. 2, this period exceeds the value of the actual period by a larger amount the smaller the parameter $\beta(\varphi) \tan \varphi$.

In the work of Eckstein et al.^[15], a divergence was observed between the experimental and theoretical values of the periods of geometric resonance in an oblique magnetic field (see the curve Δ_1^h in Fig. 2 of^[15]). Evidently the authors observed not a geometric resonance but a diffused resonance line at the boundary cross section in a weak magnetic field. A similar set of periods is shown in our Fig. 6a by the lower experimental curve.

What is not clear from the quadratic model is the presence of two closely situated split peaks in the range of angles $15-30^\circ$, having the same anisotropy (Fig. 6b). Their appearance can evidently be explained if we assume that the hole surface consists of three pairs of deformed ellipsoids and has a center of symmetry for each pair. (Fig. 9) The absolute values of the projections of the drift velocity in the direction of the vector \mathbf{k} will be different on the boundary cross sections (A_1, A_2 and B_1, B_2). Therefore, there are two series of Doppler split absorption lines, shifted according to the magnetic field. In a change in the angle of inclination the shifts of both series in the magnetic field should occur in the same manner.

Figure 7 shows the values of the cyclotron masses on the boundary cross sections. It is interesting to compare these results with the cyclotron masses at the extremal cross sections, which have been obtained experimentally from electromagnetic cyclotron resonance.^[14] In the case of the correct ellipsoidal Fermi surface, the cyclotron mass does not depend on the projection of the momentum p_z , and its value for all cross sections is the same. Comparison shows (Figs. 7a, b) that there is a quantitative divergence which exceeds the experimental errors. On the other hand, the anisotropy of the cyclotron masses on the boundary cross sections qualitatively preserves the form inherent in the ellipsoidal model (solid curves), violating this only in specific directions (for example, the sharp increase in the cyclotron mass in the XY plane in the region of angles $40-43^\circ$ in Fig. 7b). All this supports the conclusion that the Fermi surface of antimony is a set of deformed ellipsoids.

Similar conclusions can be drawn as a result of comparison of experimental and computed values for the mean drift velocities of the electrons $\bar{v}_z(p_g)$. Here there is also qualitative agreement over a broad range of angles. The existence of two series of split ACR

lines for the hole ellipsoids leads to the appearance of two values of the drift velocities for a fixed direction of the magnetic field. A similar phenomenon also exists for the cyclotron mass.

Thus, although the anisotropic quadratic model of the Fermi surface of antimony is obviously only a rough approximation to the shape of the real surface, it allows us to interpret the experimental results qualitatively from the anisotropy of the periods, cyclotron masses and mean drift velocities along the magnetic field H , and to predict the shape of the ACR lines correctly.

In conclusion, we sincerely thank É. A. Kaner for his interest in the work and for useful discussions. We also express our gratitude to V. V. Vasil'chenko for preparation of the specimens.

¹A. B. Pippard, *Phil. Mag.* **2**, 1147 (1957).

²É. A. Kaner, *Zh. Eksp. Teor. Fiz.* **43**, 216 (1962) [*Sov. Phys.-JETP* **16**, 154 (1963)].

³V. L. Gurevich, *Zh. Eksp. Teor. Fiz.* **37**, 71 (1959) [*Sov. Phys.-JETP* **10**, 51 (1960)].

⁴É. A. Kaner, V. G. Peschanskiĭ and I. A. Privorotskiĭ, *Zh. Eksp. Teor. Fiz.* **40**, 214 (1961) [*Sov. Phys.-JETP* **13**, 147 (1961)].

⁵A. A. Galkin, É. A. Kaner and A. P. Korolyuk, *Dokl. Akad. Nauk SSSR* **134**, 74 (1960) [*Sov. Phys. Doklady* **5**, 1002 (1960)]; *Zh. Eksp. Teor. Fiz.* **39**, 1517 (1960) [*Sov. Phys.-JETP* **12**, 1055 (1961)].

⁶A. P. Korolyuk and L. Ya. Matsakov, *ZhETF Pis. Red.* **2**, 30 (1965) [*JETP Lett.* **2**, 18 (1965)].

⁷A. P. Korolyuk and L. Ya. Matsakov, *ibid.* **3**, 291 (1966) [**3**, 188 (1966)].

⁸Y. Eckstein, *Phys. Lett.* **20**, 142 (1966).

⁹É. A. Kaner and V. L. Fal'ko, *Phys. Stat. Sol.* **22**, 319 (1967).

¹⁰L. M. Falicov and P. J. Lin, *Phys. Rev.* **141**, 562 (1966).

¹¹L. R. Windmiller and M. G. Priestly, *Solid State Comm.* **3**, 199 (1965).

¹²A. P. Korolyuk and L. Ya. Matsakov, *Zh. Eksp. Teor. Fiz.* **52**, 415 (1967) [*Sov. Phys. JETP* **25**, 270 (1967)].

¹³A. P. Korolyuk and L. Ya. Matsakov, *PTÉ* No. 5, 217 (1965).

¹⁴W. R. Datars and J. Wanderkooy, *IBM J. Res. Develop.* **8**, 247 (1964).

¹⁵Y. Eckstein, J. B. Ketterson and S. G. Eckstein, *Phys. Rev.* **135**, A470 (1964).

Translated by R. T. Beyer

1